von Freyberg, Axel ; Fischer, Andreas

Holistic approximation of combined surface data

Journal Article as: peer-reviewed accepted version (Postprint)

DOI of this document*(secondary publication): https://doi.org/10.26092/elib/3315

Publication date of this document: 13/09/2024

* for better findability or for reliable citation

Recommended Citation (primary publication/Version of Record) incl. DOI:

Axel von Freyberg, Andreas Fischer, Holistic approximation of combined surface data, Precision Engineering, Volume 54, 2018, Pages 396-402, ISSN 0141-6359, https://doi.org/10.1016/j.precisioneng.2018.07.009.

Holistic approximation of combined surface data☆

Axel von Freyberg*, Andreas Fischer

University of Bremen, Bremen Institute for Metrology, Automation and Quality Science (BIMAQ), Linzer Str. 13, 28359 Bremen, Germany

ARTICLE INFO

Keywords:
Holistic approximation
Dimensional metrology
Micro-production
Geometric decomposition

ABSTRACT

Modern micro-production processes demand fast and robust inspection techniques up to 100% inspection rates. For instance, a fast acquisition of the objects surface in the needed precision and density can be realized by optical measurement systems. In order to extract the relevant geometric quantities from the surface data of prismatic workpieces, the measured data points need to be assigned to the nominal geometric primitives, e. g. cylinder, plane or sphere. For this purpose, an automatable algorithm is desired, which assigns all measured points to the corresponding geometric elements and minimizes the measurement uncertainty. Such an optimal segmentation routine of combined geometric data can either be performed by rating neighboring measurement points based on their curvature or by a holistic approximation. Whereas the first approach is sensitive to noisy data and not able to distinguish between spheres and cylinders with certain radii, the holistic approximation in combination with further statistical methods promises an automatic detection of outliers.

In order to analyze the achievable measurement uncertainty with the holistic approximation approach for an object geometry composed by three-dimensional base elements (cylinder, torus, plane), the method is applied to determine the geometric features of micro deep-drawing dies. For verification, the measured geometry of the object is simulated including uniformly distributed noise within a range of ± 2.5 µm. As a result, the determined radius of the cylinder (defined to 412 µm) has a standard uncertainty due to random errors below 11 nm and an uncertainty due to systematic errors less than 1.1 nm. Furthermore, real tactile measurement data are evaluated to validate the holistic approximation. In comparison to certified analysis software, which requires a manual segmentation, the results show differences below 0.25 µm for the cylinder diameter. The increased measurement deviations are caused by assumptions of the model-based evaluation, which is essential for the automated data processing. However, the achievable uncertainty qualifies the holistic approximation for a robust and automated evaluation of geometric tolerances in the field of micro-production.

1. Introduction and state of the art

Modern production techniques enable the precise manufacturing of parts and, thus, promote the demand for high quality products. Proving the quality on high levels raises the requirements for both the acquisition and the evaluation of quality features. At the same time, increasing production rates demand fast and robust inspection techniques. Even in mass production, the trend goes towards a 100% inspection rate. The field of micro-production additionally increases the requirements for measurement systems due to the handling and the fragility of micro products. A general challenge are size effects [1], which exemplary occur on a physical-technical level by an increased ratio of surface to volume [2]. Especially the material properties are changing with decreasing dimensions. In micro-forming, for example, under certain boundary conditions the process forces increase with the grain size [3]. This is in contrast to the theory of metal forming in macro dimensions (Hall-Petch-relation) [4]. Therefore, not only the geometric inspection of the produced parts is important, but also the dimensional characterization of micro-forming tools in order to analyze process mechanisms and to optimize friction effects. Furthermore, an automated characterization of geometric features is also important for a closed-loop control of micro-production processes [5].

In terms of dimensional metrology, a fast acquisition of the parts surface in the needed precision and density can only be realized by optical measurement systems. Several measuring approaches exist, but the automatic data evaluation is still challenging. The methods can be roughly divided into 3 fields of application:

1. The evaluation of free-form surfaces, which requires a registration of the measured points to a reference model, e. g. by the Iterative

☆ This paper was recommended by Associate Editor Han Haitjema.

* Corresponding author.
E-mail addresses: a.freyberg@bimaq.de (A. von Freyberg), andreas.fischer@bimaq.de (A. Fischer).

Closest Point (ICP) algorithm [6], and a comparison to the nominal or CAD data. A good survey regarding the metrology of freeform shaped parts is summarized in Ref. [7].
2. The separation of different orders of shape deviations for data acquired by high definition metrology. For example, entropy, contrast and correlation techniques [8] or shearlet-based methods [9] can be used to separate roughness, waviness and form portions of a technical surface.
3. The evaluation of prismatic workpieces, which requires an assignment of the actual measurands to the nominal geometric primitives, e. g. cylinder, plane, sphere and torus.

The application of this work is related to the third field. Therefore, the following paragraphs focus on methods to assign the measured points to geometric objects.

In macro dimensions, the assignment is often performed by using the nominal data and an alignment of the measured points. This is a standard procedure and part of the measurement strategy [10], especially for tactile measuring systems. In most practical applications, this procedure implies neglecting points close to edges of the feature or in the area of intersecting elements. Depending on the number of measured points, which can be rather low for micro-features, and the fraction of the measured feature (Fig. 1), the minimal achievable measurement uncertainty is not attained [10–13].

The example in Table 1 illustrates the increasing uncertainties of the center and the diameter of a circle, respectively, with decreasing acquired points on the full circumference. The second example in Fig. 1 demonstrates the further increasing diameter uncertainty with decreasing central angle of the arc, on which 12 acquired points are distributed.

In addition, Fig. 2 demonstrates the effect of wrongly assigned points: The measuring data of a cross section is simulated for a micro feature (combination of a line, a circle and another line), acquired with 25 points per mm. In this dimensions, a quarter of a circle (radius r = 153.0 µm) is acquired with only 6 points. With a simulated uncertainty (uniformly distributed noise in normal direction within a range of 0.9 µm) the approximation of all 6 acquired circle points delivers a radius of 152.8 µm whereas a circle approximation of the 6 circle points together with a neighboring point on each of the lines calculates a radius of 155.0 µm. As a result, the approximation of the correct points leads to a measurement deviation (to the nominal value) of 0.2 µm, whereas the inclusion of only 2 wrongly assigned points increases the deviation by one decade. Thus, for a fast production of high quality micro products, an automated procedure is necessary, which optimally assigns all measured points to the corresponding geometric elements.

Two approaches exist for a general automated segmentation of combined geometric data:

Table 1
Uncertainties U_x, U_D (confidence level P = 95%) for the center and the diameter, respectively, approximated for different numbers of equidistant points n on a full circle, valid for independent and uniformly distributed deviations, normalized to the standard deviation s = 1 [12].

points n	Center U_x/s	Diameter U_D/s	Points n	Center U_x/s	Diameter U_D/s
4	8.98	12.70	20	0.67	0.95
5	2.72	3.85	50	0.40	0.57
6	1.84	2.60	100	0.28	0.40
10	1.06	1.50	1000	0.09	0.13

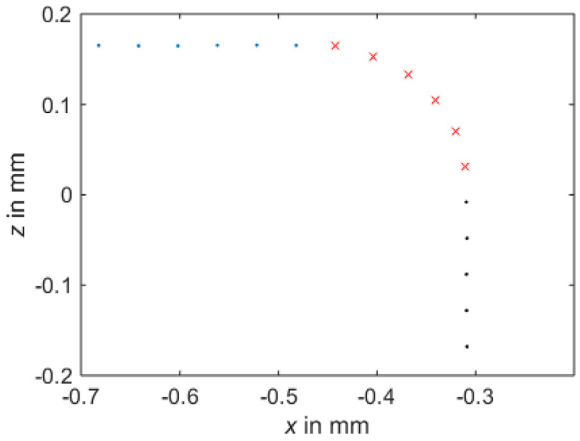

Fig. 2. Simulated measuring data of a profile, combined of a line (dots), a quarter circle (radius: 153 µm, crosses) and another line (dots), acquired with 25 points per mm.

1. Methods for the reverse engineering of unknown surfaces,
2. Model-based approaches for geometric feature extraction.

In the first field, the methods can be divided into edge-based or face-based methods. A good summary is provided in Ref. [14]. One example is rating neighboring measurement points based on their curvature and assigning them to corresponding geometric elements [15]. This method can provide very accurate solutions under certain conditions, but it is sensitive to noisy data and not able to distinguish between spheres and cylinders with certain radii.

In the second field, a model-based holistic approximation can evaluate a composed set of data in a single approximation task [16]. By the definition of separating functions, an optimal assignment of the measurement points to the corresponding geometric elements (segmentation) can be carried out simultaneously. The application for a planar line-circle-line profile is presented in Ref. [17]. A 3D application to evaluate the geometry of micro deep-drawing punches as a

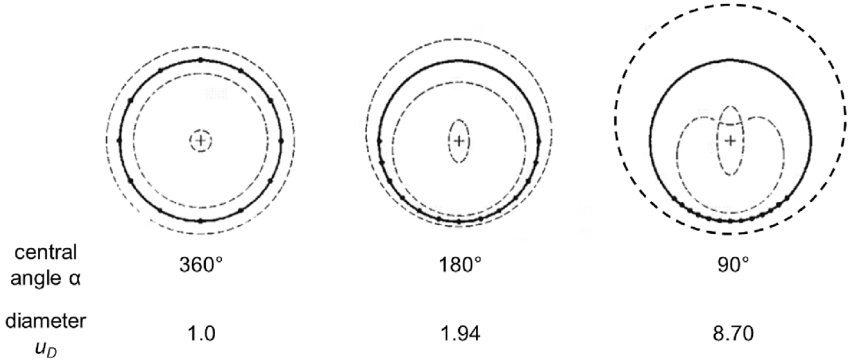

Fig. 1. Uncertainty u_D of the approximated circle diameter depending on the distribution of 12 points on the circumference normalized by the uncertainty for a fully acquired circle (α = 360°) [12].

composition of a cylinder, a torus and a plane is presented in Ref. [18], and an application for the automatic evaluation of involute gears flanks is described in Ref. [19]. A combination with statistical methods also enables the automatic detection of outliers [20], which particularly qualifies this method for the evaluation of noisy optical data. Compared to other approaches, like the point to surface assignment of planes of a hexahedron by bounding boxes [21], the holistic approximation is a universal approach, which is, in general, neither limited to special applications nor geometric object classes.

While the holistic approximation was implemented and evaluated in terms of stability and convergence, depending on the start-solution, the assessment of the uncertainty of the approximated parameters for micro features is still pending. For this reason, the aim of the article is to characterize the uncertainty of geometric features of micro deep-drawing dies, evaluated in 3D for the first time with the holistic approximation. Section 2 introduces the method and the application. In section 3, the results of the verification are presented, and in section 4 the approach is validated by means of experimental data and a reference evaluation. Section 5 closes the article with a conclusion and an outlook.

2. Method and application

Deep-drawing is a manufacturing process in which one part of the tool (punch) draws sheet material into the borehole of another tool part (drawing die) [22]. In micro production, several geometric features of these two tool parts influence the quality of the product as well as the boundaries of the process [23,24]. Due to the tool dimensions of a micro deep-drawing die (outer diameter: ca. 40 mm), the handling and the tactile measurement (see Fig. 3) can be performed with state of the art methods. Therefore, the measurement and evaluation of geometric features of this tool is an adequate application to analyze and validate the holistic approximation in terms of the achievable measurement uncertainty.

The surface to be characterized is a combination of a cylinder with radius r_c, a (quarter) torus with wall radius r_w and a plane. A cross section of the axially symmetric tool is presented in Fig. 4.

The detailed principle of the holistic approximation is described in Refs. [16–18]. For the combination of cylinder, torus and plane, the approximation is performed by minimizing the L2-Norm

$$\min_{\vec{a}_p,\,\vec{a}_g}\left[\sum_{i=1}^{n_{cyl}}(d_{i,cyl})^2+\sum_{i=1}^{n_{tor}}(d_{i,tor})^2+\sum_{i=1}^{n_{pla}}(d_{i,pla})^2\right]^{\frac{1}{2}}, \tag{1}$$

where n_{cyl}, n_{tor} and n_{pla} are the numbers of points assigned to the cylinder, the torus and the plane, respectively. A single point has the index i, and its orthogonal distance to the assigned geometric element is d_i. During the approximation, not only the degrees of freedom

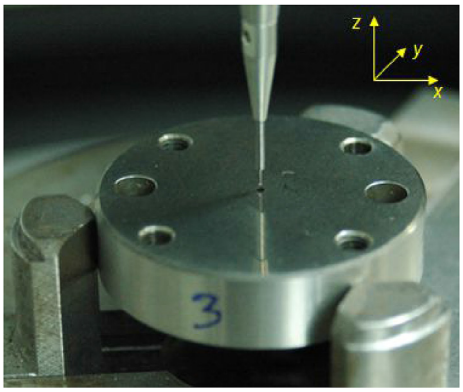

Fig. 3. Micro deep-drawing die with borehole radius $r_c < 0.5$ mm during a tactile measuring process with a ball probe (diameter: 0.6 mm).

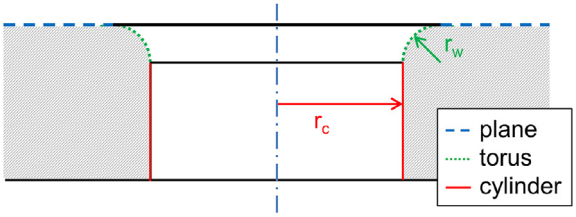

Fig. 4. Cross section of deep-drawing tool with cylindrical borehole with radius r_c and drawing edge with radius r_w.

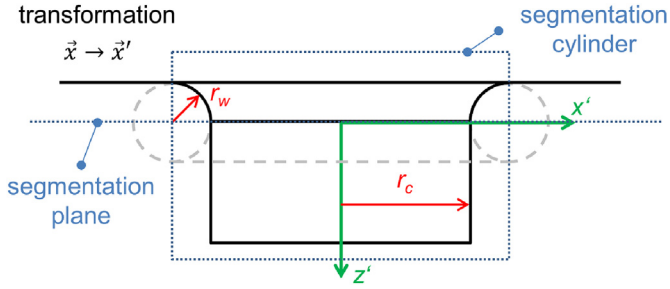

Fig. 5. Drawing die composed from geometric primitives in the workpiece coordinate system (WCS) with segmentation elements according to the geometric model.

(transformation $\vec{a}_p$ and shape parameters $\vec{a}_g$) are optimized, but also the assignment of the measurement points to the geometric elements. That implies that the numbers of elements in Eq. (1) are varying during the iterative calculation. The geometric assignment itself is based on a geometric model, which is presented in Fig. 5. It consists of a cylinder with radius r_c, whose axis represents the z-axis, a torus in the x-y-plane with wall radius r_w and ring radius $r_r = r_c + r_w$ as well as a plane parallel to the x-y-plane at $z = -r_w$. This model contains certain geometric constraints, e. g. a coaxiality of the cylinder and the torus axis, which are again perpendicular to the plane, as well as tangential transitions between all elements. These constraints result from the workpiece design and reduce the degrees of freedom to five transformation parameters $\vec{a}_p = [\Delta x, \Delta y, \Delta z, \varphi_x, \varphi_y]$ and two shape parameters $\vec{a}_g = [r_c, r_w]$. As the geometry is axially symmetric, the rotation φ_z around the z-axis remains disregarded.

Out of the geometric model, the decision rules shown in Fig. 6 are derived and implemented in the algorithm. All transformed points with a positive z-coordinate belong to the cylinder. The remaining points are distinguished by their polar radius, points with a radius $r_i > (r_c + r_w)$ are assigned to the plane, and the residual points are assigned to the torus.

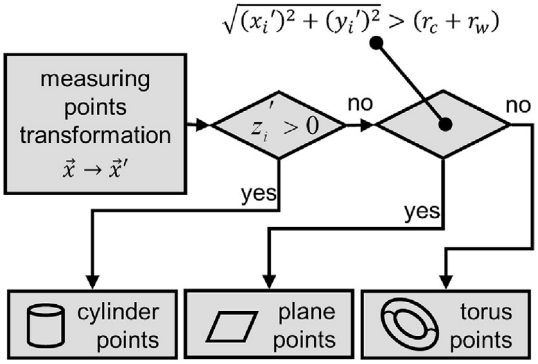

Fig. 6. Decision rules for assigning the measured points to the geometric primitives.

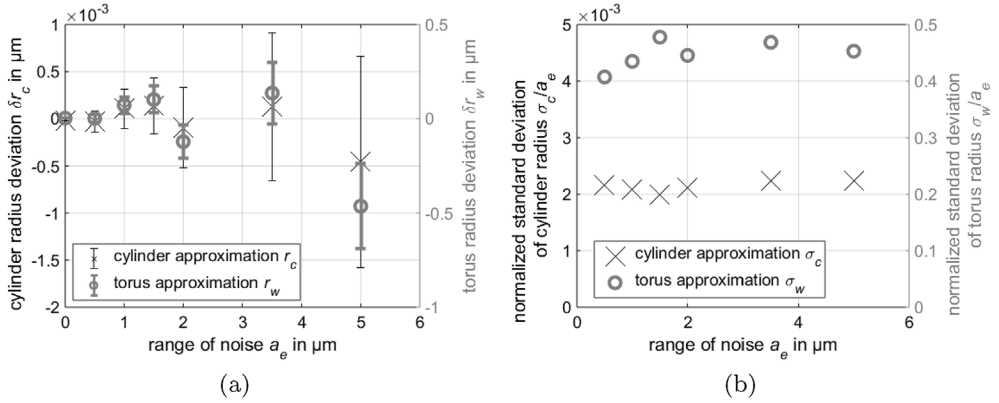

Fig. 7. Approximation results for simulated data with different ranges of noise a_e: a) mean values of the radius deviations for cylinder $\delta r_c = r_c - r_{c,0}$ and torus $\delta r_w = r_w - r_{w,0}$ with standard errors; b) standard deviations of the approximated radii of cylinder σ_c and torus σ_w, normalized by the ranges of noise a_e.

3. Verification

For the verification of the algorithms, the geometry of the measuring object was simulated as a combination of a cylinder, a torus and a plane. The cylinder radius was defined to $r_{c,0} = 412$ µm and the wall radius of the torus was $r_{w,0} = 126$ µm. These dimensions were chosen according to the application. The cylinder was formed by 300,000 equidistant points, the torus by approximately 100,000 points and the plane by 379,000 points. All three elements were superimposed with a uniformly distributed noise in normal direction of the nominal surface with different ranges $[-a_e/2, a_e/2]$ in seven steps between $a_e = 0.0...5.0$ µm. Each case was simulated $n = 100$ times and automatically evaluated by the holistic approximation. The results of the holistic approximation of the simulated data are presented in Fig. 7.

To analyze systematic deviations, a one sample t-test is performed with the hypothesis that the approximated radii are equal to the simulated values ($\delta r_c = r_c - r_{c,0} = 0$ and $\delta r_w = r_w - r_{w,0} = 0$). The required coverage factors

$$t_c = \frac{\overline{\delta r_c} \cdot \sqrt{n}}{\sigma_c}, \; t_w = \frac{\overline{\delta r_w} \cdot \sqrt{n}}{\sigma_w} \tag{2}$$

are calculated for the mean radius deviations $\overline{\delta r_c} = \bar{r}_c - r_{c,0}$ and $\overline{\delta r_w} = \bar{r}_w - r_{w,0}$, respectively, based on the mean approximated radii of the cylinder $\bar{r}_c$ and the torus $\bar{r}_w$. The maximum value for the cylinder radius is $t_{c,max} = 0.48$, whereas it is $t_{w,max} = 2.05$ for the torus radius. According to the t-distribution for a probability of 98% ($\alpha = 0.02$) and a degree of freedom of $f = n - 1 = 99$, the critical value is $t_{crit} = 2.364$. As both calculated coverage factors are below this critical value, it can be stated that the verification results dont disagree the hypothesis with a probability of error of 2%. Thus, it can be assumed that no systematic influence within the holistic approximation leads to significant deviations of both approximated radii.

The random deviations can be characterized by the standard deviations of the calculated radii. Fig. 7 b shows the standard deviations of the approximated cylinder and torus radii, σ_c and σ_w, respectively, normalized by the ranges of noise a_e. It can be clearly seen that the normalized standard deviations are nearly constant, which means the uncertainty of the algorithm is directly scaled by the range of uniformly distributed noise. The random deviations of the torus are 2 orders of magnitude higher than those of the cylinder radius. One part of this increased uncertainty of the torus radius can be explained by theoretically increased uncertainties for the approximation of partial geometric objects [10–13]. The theoretical example in Fig. 1 estimates a factor of 8.7 for the uncertainty of the radius of a quarter circle compared to a full circle. Other reasons for the increased standard deviation of the torus radius are the number of evaluated points and effects of non-optimal segmentation. The torus was simulated with approximately 100,000 points, which is only a third of the number of points on the cylinder. Therefore, the relation between a certain number of wrongly assigned points and the total number of points for the torus is higher than for the cylinder. As a result, the determination of the torus radius is more sensitive to wrongly assigned points than the determination of the cylinder radius. This sensitivity of the torus radius is also confirmed by the results of the manual reference torus evaluation (cf. Fig. 9), whose standard deviation $\sigma_{r,w} = 15.8$ µm is two orders of magnitude higher than the certified uncertainty of the cylinder radius reference evaluation (0.1 µm). Nevertheless, for both parameters the standard deviation is only a fraction of the initial amplitude of noise. In absolute numbers, the standard deviation of the cylinder radius is $\sigma_c < 11$ nm in this simulation, while the standard deviation of the torus radius is $\sigma_w < 2.26$ µm.

4. Validation with experimental data

The experimental data [dataset] [25] for validating the algorithms was acquired with a coordinate measuring machine (CMM) with a maximum permissible volumetric probing error of $P_{MPE} = 0.9$ µm, using a probe with 600 µm diameter. A CMM was used, as no traceable optical measurement system is available at the moment to acquire the surface with a comparable low uncertainty. The measurement procedure is shown in Fig. 3. At five different tools with nominal borehole diameters between 820 and 870 µm and die radii between 0 and 300 µm, 72 cross section profiles in planes parallel z were measured in scanning modus with a point density of 500 points/mm, resulting in approximately 122,000 measured points in total.

The measured data was evaluated in two ways, by the holistic approximation and as reference manually by means of certified analysis software (GeoMagic Control 2015.0.0.194), respectively. Within the reference software, the cylinder points have to be selected manually prior to the approximations (Fig. 8). The processing time of one dataset takes a few seconds with the holistic approximation and can be reduced to 0.25 s under certain conditions, whereas it takes several minutes with the reference software due to the manual interaction. As the reference software does not provide the possibility to approximate a torus, the radius of the circle was measured in 4 cross sections. The measurement was repeated 10 times in each cross section, because the circle radius is quite sensitive with respect to the manual selection of the circle points (see Fig. 9).

For the reference software, the numerical uncertainty of an approximated cylinder radius is certified by the German National Metrology Institute (PTB, Physikalisch-Technische Bundesanstalt) below 0.1 µm. A torus approximation is not provided, but the wall radius of the torus can be estimated by a circle approximation in a cross section. The maximum standard deviation of the reference torus radius was estimated to $\sigma_{r,w} = 15.8$ µm, resulting from the manual measurements in 4 cross-sections per tool each with 10 repetitions.

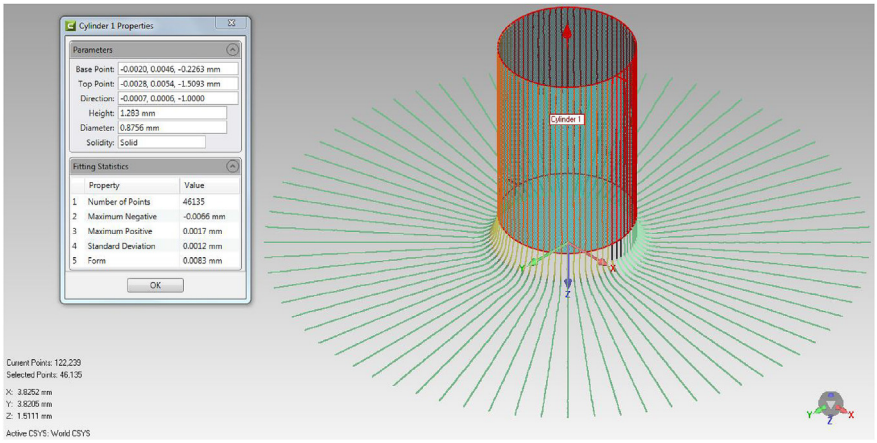

Fig. 8. Cylinder approximation with reference software after manual segmentation (tool number 4).

The results of the holistic approximation are presented in Fig. 10 in comparison to the reference evaluation. In order to analyze systematic influences for the cylinder evaluation, the deviations between the holistic approximated radii and those evaluated with the reference software are compared to the uncertainties of both algorithms. The uncertainty of the holistic approximation is estimated by the standard deviation $\sigma_c = 2.1$ nm for the cylinder approximation of simulated data for a range of noise of 1 µm, which corresponds to the probing error of the used CMM. Taking into account the certified uncertainty of the reference evaluation (0.1 µm), the residual deviations of up to 0.15 µm can not be explained by the confidence interval resulting from σ_c and a coverage factor $k = 3$ for 4 out of 5 measured data sets. Although all deviations are below 0.25 µm, the majority of the results do not agree with a high statistical probability. Thus, the holistic approximation of the cylinder radius contains systematic deviations, which are mainly caused by the geometric modelling. The explanation is provided by an example at the end of this section.

In order to analyze the systematic influences for the torus evaluation, the deviations between the holistic approximated radii and those evaluated with the reference software are again compared to the uncertainties of both algorithms. As the results are not as obvious as for the cylinder radius, a two-sample means test with inhomogeneous variances [26] was performed in this case. The error bars of the torus radius deviations Δr_w in Fig. 10 represent the confidence interval $[-U, U]$, with

$$U = \sqrt{\frac{\sigma_w^2}{n_h} + \frac{\sigma_{r,w}^2}{n_r}} \cdot t \tag{3}$$

for a significance level of 95%. Here, $\sigma_w = 0.4$ µm is the standard deviation for the holistic approximation (estimated from $n_h = 100$ simulations with a noise range $a_e = 1$ µm), $\sigma_{r,w}$ is the standard deviation of the reference torus radius, n_r the number of manual measurements in the reference software and t is the coverage factor of the t-distribution (degree of freedom: 39). It can be clearly seen in Fig. 10 that the case of

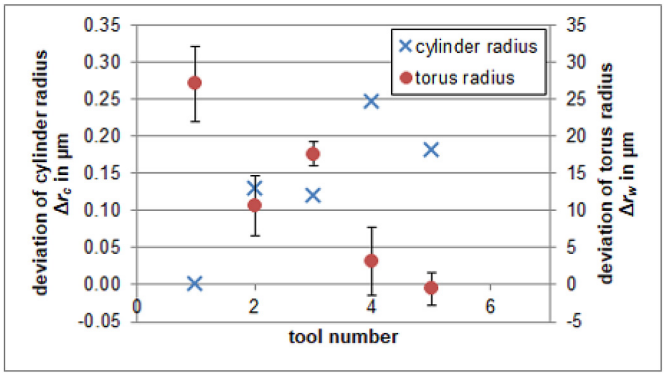

Fig. 10. Deviations of cylinder radius Δr_c and torus radius Δr_w, evaluated with the holistic approximation compared to the reference software results. The error bars of the torus radius represent the confidence interval $[-U, U]$ according to equation (3).

no deviation ($\Delta r_w = 0$ µm) is only included in 2 out of 5 tool measurements. Thus, also the holistic approximation results for the torus radius do not agree in all cases with the reference evaluation. The causes for these large deviations are again systematic effects, but in both evaluations (holistic approximation as well as reference software). The systematic effects are partly visible in Fig. 9. On the one hand, the torus shows a certain shape deviation, which leads to different radii in different cross sections. On the other hand, the approximation of a partial feature (quadrant) is afflicted with an increased uncertainty, which is confirmed by the increased standard deviation of the manual reference circle (torus cross-section) measurements.

In general, the raised deviations compared to the simulative verification are mainly caused by

- deviations between the real surface and the geometric model (nominal geometry),

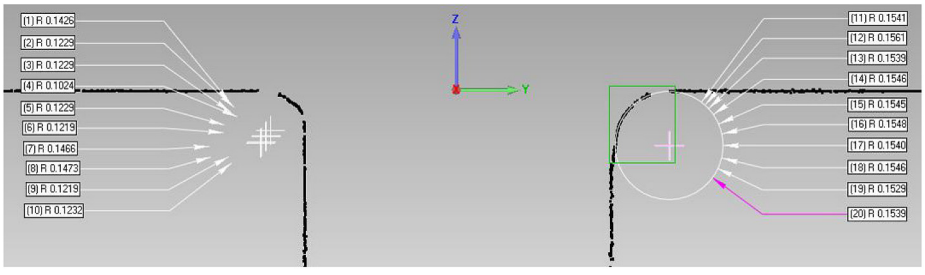

Fig. 9. Repeated manual circle approximation in 2 cross sections within the y-z-plane with the reference software (tool number 4).

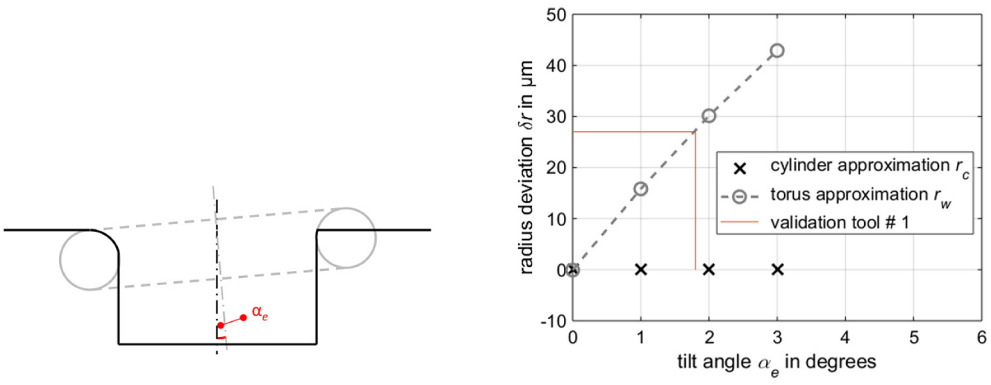

Fig. 11. Effect of coaxiality deviations between cylinder and torus: a) visualization of coaxiality, characterized by the tilt angle α_e; b) holistic approximation results for different tilt angles α_e, simulated with a noise range $a_e = 1.0$ µm.

- the additional numerical uncertainty of the values calculated by the reference software.

The first effect is a systematic influence and can be illustrated by the following example: The geometric model is based on the design specifications and assumes a coaxiality of cylinder and torus. If the production process of the workpiece delivers an increased coaxiality deviation (cf. Fig. 11 a), the degrees of freedom of the holistic approximation do not allow a certain shift or tilting of the combined objects. Therefore, the ideal alignment leads to higher residual distances of both (combined) objects, weighted by the numbers of points assigned to each of the objects. The number of points assigned to the cylinder is about 50,000, and the number of torus points is about 23,000. An increasing torus radius deviation for increasing tilt angles α_e is visible in Fig. 11 b as a result of a holistic approximation of simulated data with a noise range $a_e = 1.0$ µm. In the same simulation, no significant influence can be observed for the cylinder radius. The maximum torus radius deviation of 27.1 µm within the validation (cf. tool number 1 in Fig. 10) can be explained by the almost linear relation in Fig. 11 b with a tilt angle $\alpha_e = 1.8°$. Thus, it is reasonable to quantitatively explain the higher systematic deviation of the torus radius compared to the cylinder radius by a coaxiality deviation.

5. Conclusion and outlook

This contribution characterizes the uncertainty of geometric features of micro deep-drawing dies, evaluated in 3D for the first time with the holistic approximation. The holistic approximation allows for an automated dimensional analysis of prismatic surface data, whereat the surface can be a combination of different simple geometric base bodies (like cylinder, plane, torus, etc.). The assignment of the measured points to the corresponding objects is based on a parametric geometry model, which defines the degrees of freedom of the least-squares approximation. Processing times down to 0.25 s can be reached with the holistic evaluation, enabling the inspection of up to 240 parts per minute.

The verification of the holistic approximation was successful. As a result, the radius of the cylinder (defined to 412 µm) has a standard uncertainty due to random errors below 11 nm and a standard error due to systematic effects less than 1.1 nm. The uncertainties of the torus are higher due to a smaller number of points and the fact that the element is incomplete. Furthermore, real tactile measurement data was evaluated with the holistic approximation. In comparison to certified analysis software, which requires a manual segmentation, the results show differences below 0.25 µm for the cylinder diameter and up to 27 µm for the torus wall diameter. The increased measurement deviations compared to the verification with simulated data are systematic effects and mainly caused by the assumptions of the model-based evaluation, which is essential for an automated data processing. However, the geometric model could be adapted to the boundary conditions, if meaningful. In this case, it has to be proven individually whether an increased number of degrees of freedom decreases the uncertainty, as a higher number of free parameters could otherwise negatively affect the convergence of the algorithms. Essentially, the proven achievable uncertainty validates the holistic approximation for a robust and automated evaluation of geometric tolerances in the field of micro-production.

The actual implementation of the holistic approximation limits the evaluation to combinations of geometric base bodies, e. g. plane, sphere, cylinder, torus. The future evaluation of combined complex geometries, e. g. ellipses, parables or other implicitly formulated objects, requires an extension by a root point iteration [27]. Furthermore, an approximation by the maximum norm can be implemented [28] to evaluate shape deviations of the individual geometric elements.

Acknowledgment

The authors gratefully acknowledge the financial support by Deutsche Forschungsgemeinschaft (DFG, German Research Foundation) for Subproject B5 “Sichere Prozesse” within the SFB 747 (Collaborative Research Center) “Mikrokaltumformen - Prozesse, Charakterisierung, Optimierung”.

Appendix A. Supplementary data

Supplementary data related to this article can be found at https://doi.org/10.1016/j.precisioneng.2018.07.009.

References

[1] Raulea L, Goijaerts A, Govaert L, Baaijens F. Size effects in the processing of thin metal sheets. J Mater Process Technol 2001;115(1):44–8.
[2] Vollertsen F, Biermann D, Hansen HN, Jawahir I, Kuzman K. Size effects in manufacturing of metallic components. CIRP Ann Manuf Technol 2009;58(2):566–87.
[3] Geiger M, Kleiner M, Eckstein R, Tiesler N, Engel U. Microforming. CIRP Ann Manuf Technol 2001;50(2):445–62.
[4] Petch N. The cleavage strength of polycrystals. J Iron Steel Inst 1953:25–8.
[5] Zhang P, von Freyberg A, Fischer A. Closed-loop quality control system for laser chemical machining in metal micro-production. Int J Adv Manuf Technol 2017;93(9–12):3693–703.
[6] Besl PJ, McKay ND. A method for registration of 3-d shapes. IEEE Trans Pattern Anal Mach Intell 1992;14(2):239–56.
[7] Savio E, De Chiffre L, Schmitt R. Metrology of freeform shaped parts. CIRP Ann Manuf Technol 2007;56(2):810–35.
[8] Wang M, Xi L, Du S. 3d surface form error evaluation using high definition metrology. Precis Eng 2014;38(1):230–6https://doi.org/10.1016/j.precisioneng.2013.

08.008http://www.sciencedirect.com/science/article/pii/S014163591300144X.
[9] Du S, Liu C, Huang D. A shearlet-based separation method of 3d engineering surface using high definition metrology. Precis Eng 2015;40:55–73https://doi.org/10.1016/j.precisioneng.2014.10.004http://www.sciencedirect.com/science/article/pii/S0141635914001603.
[10] D. Flack, Measurement good practice guide no. 41: Cmm measurement strategies, National Physical Laboratory, London, UK.
[11] Bourdet P, Lartigue C, Leveaux F. Effects of data point distribution and mathematical model on finding the best-fit sphere to data. Precis Eng 1993;15(3):150–7.
[12] Hernla M. Abschätzung der Messunsicherheit bei Koordinatenmessungen unter den Bedingungen der industriellen Fertigung. VDI-Verlag; 1992.
[13] McCool J. Systematic and random errors in least squares estimation for circular contours. Precis Eng 1979;1(4):215–20.
[14] Vrady T, Martin RR, Cox J. Reverse engineering of geometric models–an introduction. Comput Aided Des 1997;29(4):255–68. reverse Engineering of Geometric Models https://doi.org/10.1016/S0010-4485(96)00054-1http://www.sciencedirect.com/science/article/pii/S0010448596000541.
[15] Westkämper E, Stotz M, Effenberger I. Automatic segmentation of measurement point clouds to geometric primitives. TM Tech Mess 2006;73:60–6https://www.degruyter.com/view/j/teme.2006.73.issue-1_2006/teme.2006.73.1.60/teme.2006.73.1.60.xml.
[16] Goch G. Algorithm for the combined approximation of continuously differentiable profiles composed of straight lines and circle segments. Ann CIRP 1991;40/I:499–502.
[17] Lübke K, Sun Z, Goch G. Ganzheitliche approximation eines gerade-kreis-gerade-profils mit automatischer trennung in einzelprofile. In: Scholl G, editor. XXIV. Messtechnisches Symposium des Arbeitskreises der Hochschullehrer für Messtechnik e.V. AHMT); 2010. p. 77–90.
[18] Lübke K, Sun Z, Goch G. Three-dimensional holistic approximation of measured points combined with an automatic separation algorithm. CIRP Ann Manuf Technol 2012;61(1):499–502.
[19] von Freyberg A, Fischer A. Automatic geometry segmentation of involute flank regions. International conference on gears 2017, no. 2294 in VDI-Berichte, VDI-society for product and process design. VDI-Verlag GmbH; 2017. p. 1015–24.
[20] Grubbs FE. Procedures for detecting outlying observations in samples. Technometrics 1969;11(1):1–21.
[21] Shin D, Kurfess TR. Three-dimensional metrology of surface extracted from a cloud of measured points using a new point-to-surface assignment method: an application to pcb-mounted solder pastes. Precis Eng 2004;28(3):302–13.
[22] Vollertsen F, Hu Z, Schulze-Niehoff H, Theiler C. State of the art in micro forming and investigations into micro deep drawing. J Mater Process Technol 2004;151(1–3):70–9.
[23] Behrens G, Vollertsen F. Influence of tool geometry variation on the punch force in micro deep drawing. Key engineering materials, vol. 554. Trans Tech Publ; 2013. p. 1306–11.
[24] Behrens G, Trier F, Tetzel H, Vollertsen F. Influence of tool geometry variations on the limiting drawing ratio in micro deep drawing. Int J Mater Form 2016;9(2):253–8.
[25] von Freyberg A. Measurement data of drawing dies vol. 1. Mendeley Data; Mar. 2018. https://doi.org/10.17632/xc7xmz22jj.1.
[26] Moser BK, Stevens GR. Homogeneity of variance in the two-sample means test. Am Statistician 1992;46(1):19–21.
[27] Ahn SJ, Rauh W, Recknagel M. Least squares orthogonal distance fitting of implicit curves and surfaces. Pattern recognition: 23rd DAGM symposium, Munich, Germany, September 12-14, 2001. Proceedings. 2001. p. 398–405.
[28] Goch G, Lübke K. Tschebyscheff approximation for the calculation of maximum inscribed/minimum circumscribed geometry elements and form deviations. CIRP Ann Manuf Technol 2008;57(1):517–20.